The Stacking Tryptophan of Galactose Oxidase: A Second-Coordination Sphere Residue that Has Profound Effects on Tyrosyl Radical Behavior and Enzyme Catalysis[†,‡]

Melanie S. Rogers,[§] Ejan M. Tyler,[§] Nana Akyumani,[∥] Christian R. Kurtis,[∥] R. Kate Spooner,[∥] Sarah E. Deacon,[∥] Sarita Tamber,[∥] Susan J. Firbank,[∥] Khaled Mahmoud,[∥] Peter F. Knowles,[∥] Simon E. V. Phillips,[∥] Michael J. McPherson,*[,∥] and David M. Dooley*[,§]

Department of Chemistry and Biochemistry, Montana State University, Bozeman, Montana 59717, and Astbury Centre for Structural Molecular Biology and Institute of Molecular and Cellular Biology, University of Leeds, Leeds LS2 9JT, U.K.

Received October 13, 2006; Revised Manuscript Received January 19, 2007

ABSTRACT: The function of the stacking tryptophan, W290, a second-coordination sphere residue in galactose oxidase, has been investigated via steady-state kinetics measurements, absorption, CD and EPR spectroscopy, and X-ray crystallography of the W290F, W290G, and W290H variants. Enzymatic turnover is significantly slower in the W290 variants. The K_m for D-galactose for W290H is similar to that of the wild type, whereas the K_m is greatly elevated in W290G and W290F, suggesting a role for W290 in substrate binding and/or positioning via the NH group of the indole ring. Hydrogen bonding between W290 and azide in the wild type−azide crystal structure are consistent with this function. W290 modulates the properties and reactivity of the redox-active tyrosine radical; the Y272 tyrosyl radicals in both the W290G and W290H variants have elevated redox potentials and are highly unstable compared to the radical in W290F, which has properties similar to those of the wild-type tyrosyl radical. W290 restricts the accessibility of the Y272 radical site to solvent. Crystal structures show that Y272 is significantly more solvent exposed in the W290G variant but that W290F limits solvent access comparable to the wild-type indole side chain. Spectroscopic studies indicate that the Cu(II) ground states in the semireduced W290 variants are very similar to that of the wild-type protein. In addition, the electronic structures of W290X−azide complexes are also closely similar to the wild-type electronic structure. Azide binding and azide-mediated proton uptake by Y495 are perturbed in the variants, indicating that tryptophan also modulates the function of the catalytic base (Y495) in the wild-type enzyme. Thus, W290 plays multiple critical roles in enzyme catalysis, affecting substrate binding, the tyrosyl radical redox potential and stability, and the axial tyrosine function.

Over the past 20 years, there has been a growing appreciation for the catalytic utility of protein-derived free radical cofactors in enzymes (*1*−*3*). Free radical chemistry is harnessed to catalyze bond activation and molecular rearrangements in a wide variety of enzymes, including ribonucleotide reductase (*4*−*7*), DNA photolyase (*8*), cytochrome *c* peroxidase (*9*), pyruvate-formate lyase (*10*), lysine-2,3-aminomutase (*11*), prostaglandin H synthase (*12*), glyoxal oxidase (*13*), and galactose oxidase (*14*).

It is becoming increasingly clear that the environment of a protein-based radical can play a significant role in modulating its properties and reactivity (*15*−*18*). The case of *Escherichia coli* ribonucleotide reductase, where alteration of the hydrophobic environment of the tyrosyl radical by mutation of second-coordination sphere residues dramatically lowers radical stability, is especially pertinent (*19*, *20*). Additionally, substantial evidence now indicates that second-coordination shell effects in metalloproteins may profoundly influence the reactivity and electronic structure of active site metal ions, while weak interactions (such as hydrogen bonds) have been strategically manipulated to control reactivity in proteins and model complexes (*21*−*28*).

We have initiated a systematic investigation of the influence of the active site microenvironment on the structure and reactivity of the tyrosyl radical (Y•) in the copper radical enzyme, galactose oxidase (*29*, *30*). A notable feature of the Cu(II)-Y• active site is the presence of the so-called "stacking tryptophan", W290 (Figure 1). As presented herein, our results indicate that the second-coordination sphere residue W290 has significant effects on the generation and reactivity of the tyrosyl radical (Y272) in galactose oxidase and, consequently, the catalytic activity of the enzyme.

Galactose oxidase (secreted by *Fusarium graminearum*) contains a mononuclear copper ion coordinated to a post-translationally modified, cross-linked cysteine−tyrosine radical cofactor (Figure 1) (*31*).

[†] This work was supported by a grant from the National Institutes of Health (GM27659 to D.M.D.) and from the Biotechnology and Biological Sciences Research Council (M.J.M.). N.A. and S.J.F. thank the BBSRC for studentship awards. K.M. thanks the Egyptian Government for studentship funding.

[‡] The atomic coordinates and structure factors for W290G, W290F, and W290H have been deposited in the Protein Data Bank as entries 2EID, 2EIC, and 2EIB, respectively.

* To whom correspondence should be addressed. D.M.D.: e-mail, dmdooley@montana.edu; telephone, (406) 994-4373; fax, (406) 994-7989. M.J.M.: e-mail, m.j.mcpherson@leeds.ac.uk; telephone, +44 113 233-2595; fax, +44 113 233-3167.

[§] Montana State University.

[∥] University of Leeds.

10.1021/bi062139d CCC: $37.00 © 2007 American Chemical Society
Published on Web 03/27/2007

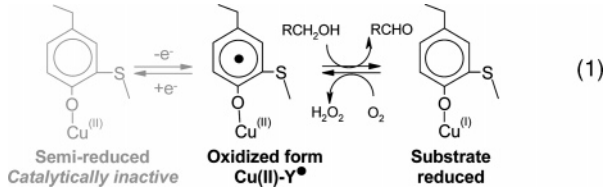

(1)

A growing number of enzymes have been found to have cofactors derived from post-translationally modified amino acids (*32*). Galactose oxidase catalyzes the stereospecific (*33*) two-electron oxidation of primary alcohol to the corresponding aldehyde, reducing O_2 to hydrogen peroxide (eq 1). The enzyme has K_M values in the millimolar range (*30*, *34*) and a broad substrate range (*35*, *36*). The precise biological roles of galactose oxidase and related enzymes are not known but may be associated with peroxide formation (*37*, *38*).

The structure of galactose oxidase has been determined by X-ray crystallography to 1.7 Å resolution (*31*, *39*) and the chemistry of its active site studied extensively. Y272, the site of the free radical in the oxidized form of galactose oxidase (*40*), is modified by a thioether cross-link to C228, and W290 "stacks" over this unit (Figure 1). In model systems, thioether substitution of the tyrosyl radical stabilizes the one-electron oxidized state by ~540 mV relative to an unsubstituted tyrosyl radical (*2*, *41*). The coordinated H_2O can be displaced by acetate and azide or by alcohol substrates, suggesting that this is the site of substrate binding (*42*). The axial ligand Y495 may act as a base to accept a proton from the bound alcohol substrate, activating the alcohol for oxidation and dissociating from the copper ion (*43*, *44*).

Previous studies had suggested that W290 influences the redox properties and reactivity of the tyrosyl radical and may play other roles in catalysis. The W290H[1] tyrosyl radical redox potential is 730 mV (*45*) compared to 430 mV in the wild-type enzyme (*41*), and the radical of W290H appears unstable at pH 7.0 (*29*, *30*). Modeling studies suggested that W290 may be involved in binding D-galactose and perhaps in stabilizing the transition state for oxidation of this substrate (*39*, *46*). W290 might also modulate the reactivity of the catalytic base, Y495 (*47*).

This paper seeks to define the role(s) of W290 in galactose oxidase by comparing the properties of the wild-type enzyme to those of three W290 mutational variants (W290F, W290H, and W290G). The crystal structures of these variant proteins have been determined, and the reactivity and electronic structure have been defined through spectroscopic and kinetic methodologies. The roles of W290 are discussed in light of these new findings.

EXPERIMENTAL PROCEDURES

Enzyme Purification. Wild-type, W290H, and W290G *F. graminearum* galactose oxidase were purified from the *Aspergillus nidulans* overexpression system (*30*). Purity and molecular weight were confirmed by SDS−PAGE. Wild-type and W290F galactose oxidase were alternatively isolated via a *Pichia pastoris* expression system (*48*, *49*). Galactose oxidase purified from the yeast expression system had kinetic and structural properties essentially indistinguishable from those of the enzyme isolated from the fungal expression system. Protein concentrations were calculated using an ϵ_{280} of 104 900 M^{-1} cm^{-1} (*50*). The concentrations of W290 variants were corrected by multiplying by $^{16}/_{15}$ to account for the lowered tryptophan content. Thioether bond formation was assessed by SDS−PAGE analysis, taking advantage of the anomalous migration characteristic of the protein with the tyrosine−cysteine cross-link (*30*).

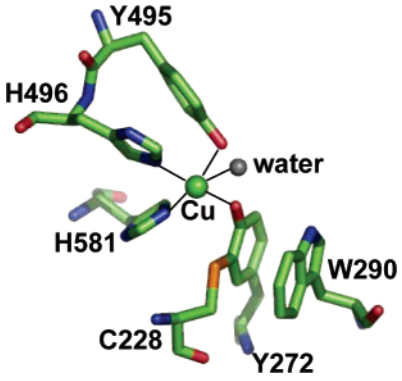

FIGURE 1: Active site of wild-type galactose oxidase at pH 7.0 (1GOG). The copper is shown as a green sphere, and the ligand bonds to the copper are shown as solid lines. Figure produced using Insight (Accelrys).

Copper Analysis by Atomic Absorption Spectrometry. The copper content of each galactose oxidase protein was analyzed using a Buck Scientific model 210VGP atomic absorption spectrophotometer. Protein samples were prepared at a concentration of 1 mg/mL using 50 mM potassium phosphate (pH 7.0) as a background control.

Enzyme Kinetics. The specific activity was determined as described previously via detection of H_2O_2 using a coupled assay (*30*). Suitably diluted enzyme was added to 1 mL of assay buffer containing 600 mM D-galactose, 0.8 mM ABTS, and 20 units/mL horseradish peroxidase (HRP) in 100 mM sodium phosphate (pH 7.0). The absorbance change at 415 nm was recorded on an HP8453 spectrophotometer at 25 °C. Specific activity was calculated from the rate of production of the ABTS radical cation (ϵ_{415} = 31 300 M^{-1} cm^{-1}) assuming two molecules of the ABTS radical cation are produced from every molecule of hydrogen peroxide (*48*). One unit of specific activity of galactose oxidase corresponds to 1 μmol of H_2O_2 produced min^{-1} mg^{-1}.

k_{cat} and K_m Determination. k_{cat} and K_m values for D-galactose were determined as previously described (*30*, *49*) via coupled specific activity assays containing HRP and ABTS, performed over a D-galactose concentration range of 2.5−907.5 mM. A substrate-depleted assay mixture was supplemented with D-galactose to the required concentration. The amount of protein present in each assay was as follows: 1.16×10^{-7} μmol for the wild type, 9.46×10^{-6} μmol for W290F, 6.8×10^{-5} μmol for W290G, and 2.88×10^{-4} μmol for W290H. Nonlinear curve fitting to the Michaelis−Menten equation was used to determine K_m and k_{cat} (OriginLab).

[1] Abbreviations: wild type, wild-type galactose oxidase; W290F, W290F galactose oxidase; W290G, W290G galactose oxidase; W290H, W290H galactose oxidase; 2MP, 2-methylene-1,3-propanediol; 8CNMO, cesium octacyanomolybdate; LMCT, ligand-to-metal charge transfer; LLCT, ligand-to-ligand charge transfer; ABTS, 2,2′-azinobis(3-ethylbenzothiazoline-6-sulfonic acid), diammonium salt; HRP, horseradish peroxidase.

Kinetic parameters for 2-methylene-1,3-propanediol (2MP) were determined via oxygen consumption assays (0.680 mL) using a Clark-type oxygen electrode (Instech). Reaction buffer [15 units/mL horseradish peroxidase in 100 mM potassium phosphate (pH 7.0)] was added to the reaction chamber, followed by substrate (from 2 to 500 mM) and finally enzyme. The amounts of protein present in these assays were as follows: 7.6×10^{-12} mol for the wild type, 6.9×10^{-12} mol for W290F, 5.13×10^{-9} mol for W290G, and 9.44×10^{-9} mol for W290H. k_{cat} and K_m were determined as described above.

X-ray Crystallographic Data Collection and Structure Determination. Crystals of W290F and W290G were grown from protein as isolated, using hanging drop vapor diffusion from 1 to 2 M $(NH_4)_2SO_4$ and 0.1 M sodium acetate at pH 4.0−5.0. To prepare the azide complex, wild-type galactose oxidase was dialyzed into 50 mM PIPES (pH 7.0) for 2 h, before addition of 20 mM sodium diethyl dithiocarbamate (DDC). The copper chelator DDC promotes the formation of orthorhombic crystals, which have more favorable crystal packing for substrate soaking experiments. The copper-free protein was crystallized in 13.5% PEG 8000, 200 mM calcium acetate, and 100 mM MES (pH 6.3). The crystals grew to full size (approximately 400 μm × 75 μm) in 2−3 weeks and were loaded with copper via addition of 250 mM copper acetate to the crystallization mother liquor for 4 h. After the sample had been washed with mother liquor to remove excess copper acetate, a suitable crystal was transferred to mother liquor containing 10 mM azide, before the transfer to a cryoprotectant comprising mother liquor, 10 mM azide, and 20% PEG 400 followed by flash-cooling in liquid nitrogen. Crystals of W290F and W290G were briefly transferred to cryoprotectant, comprising mother liquor and 25% glycerol, before being flash-cooled in liquid nitrogen. Diffraction data for all crystals were collected at 100 K on station 9.6 at the Daresbury Synchrotron Radiation Source (SRS), using an ADSC quantum IV CCD detector.

Diffraction image data for W290F and the azide complex were integrated using MOSFLM (*51*) and processed with programs from the CCP4 suite (*52*). W290F crystals diffracted to only 2.8 Å but were isomorphous with the original galactose oxidase structure (*39*), and phase information was obtained from the wild-type galactose oxidase model (1GOG) with F290 modeled as alanine. Following rigid body, positional, and *B*-factor refinement with CNS, water molecules were added, F290 was built into the model, and refinement continued until *R* equaled 17.7% and R_{free} equaled 23.3%. The wild-type azide complex crystal diffracted to 1.8 Å and was isomorphous with a previously determined orthorhombic wild-type structure (*53*). An azide ligand was added to this model at the copper site, and only minor changes to the protein and water molecules were needed before refinement to an *R* of 19.2% and an R_{free} of 20.9%. Coordination distances to copper were subjected to weak restraints to standard values in all structures.

W290G crystallized in space group $P6_522$, with a very long *c* axis, requiring the detector to be moved further from the crystal, limiting the resolution of the data to 2.2 Å. The diffraction images were integrated using the HKL suite (*54*), scaled and merged in SCALEPACK, and subsequently processed with CCP4. The structure of another variant, Y495K, that had been determined in the same crystal form (*55*) was used as a starting model, and refinement proceeded in a manner similar to that of W290F to an *R* of 19.1% and an R_{free} of 22.7%. Data collection, processing, and refinement statistics are listed in Table 1.

Table 1: Crystallographic Statistics for W290F and W290G Galactose Oxidase Variants and the Wild Type−Azide Complex

	W290G	W290F	wild type−N_3 complex
space group	$P6_522$	$C2$	$P2_12_12_1$
unit cell dimensions	$a = 89.88$ Å	$a = 97.77$ Å	$a = 59.31$ Å
	$b = 89.88$ Å	$b = 88.89$ Å	$b = 89.25$ Å
	$c = 415.33$ Å	$c = 86.19$ Å	$c = 134.37$ Å
		$\beta = 117.9°$	
resolution (Å)	10−2.2	30−2.8	39−1.8
wavelength (Å)	0.864	0.864	0.864
no. of observed reflections	33161	42956	682200
no. of unique reflections	12672	14432	65987
completeness (%)	64.6	89.3	97.0
R_{merge} (%)	7.0	8.4	4.7
R_{cryst} (%)	19.1	17.7	19.2
R_{free} (%)	22.7	23.3	20.9
no. of atoms	5341	5096	5373
rms deviation			
bond lengths (Å)	0.013	0.010	0.011
bond angles (deg)	1.60	1.55	1.62

All structures were superimposed using LSQMAN (*56*) to fit C_α atoms of the refined models for W290G, W290F, W290H, and the azide complex to the wild-type structure (1GOF). Solvent contact surface areas (in square angstroms on the van der Waals surface of protein atoms contacted by a sphere with a radius of 1.4 Å) for galactose oxidase proteins were calculated using AREAIMOL (*52*), utilizing the Lee and Richards method (*57*). Hydrogens, waters, and nonprotein atoms, but not the copper ion, were excluded from the calculation. Solvent−protein contact surface representations were produced using PyMOL (DeLano Scientific, San Carlos, CA). This is the surface traced out by the surface of a water atom (van der Waals radius of 1.4 Å) in contact with the protein molecule represented by atomic spheres with van der Waals radii.

Generation of Oxidized and Semireduced Galactose Oxidase. As isolated, galactose oxidase is a mixture of the oxidized and semireduced forms (*14*), so treatment with redox agents is required to obtain homogeneous redox states of the enzyme prior to spectroscopic experiments. Fully activated enzyme samples [Cu(II)-Y$^\bullet$] were prepared by oxidizing galactose oxidase (2 mg) with either a 500-fold excess of potassium ferricyanide ($E^{\circ\prime} = 424$ mV) (*58*) for the wild type and W290F or a 12-fold excess of cesium octacyanomolybdate (8CNMO) ($E^{\circ\prime} = 892$ mV) (*59*) for W290G and W290H variants. 8CNMO was synthesized as previously described (*29*). The concentration of 8CNMO solutions, prepared immediately before use in double-deionized water, was determined using an ϵ_{390} of 1339 M^{-1} cm^{-1}. Enzymatically inactive semireduced galactose oxidase [Cu(II)-Y] was prepared by reduction with a 500-fold excess of potassium ferrocyanide. Enzyme samples were in 100 mM potassium phosphate (pH 7.0). The oxidant or reductant was rapidly removed by gel filtration using a 10 mL Bio-Gel P-6DG column equilibrated with either 100 mM sodium phosphate (pH 7.0) or 50 mM sodium acetate (pH 4.5). Typically, the concentration of eluted protein was 15−25 μM. The time from the addition of oxidant or reductant to data collection was consistently between 2 and 3 min.

Tyrosyl Radical Decay. Oxidized galactose oxidase was prepared as described above. Following the removal of excess oxidant by gel filtration, the stability of the tyrosyl radical was measured by the decrease in absorbance at 445 nm (pH 7.0) or 455 nm (pH 4.5). The rate of radical decay was determined using nonlinear curve fitting methods (OriginLab) with the following equations: $y = A_o \exp(-kt) + A_\infty$ for the wild type, W290H, and W290G (monophasic fit) and $y = A_1 \exp(-k_1 t) + A_2 \exp(-k_2 t) + A_\infty$ for W290F (biphasic fit).

Spectroscopy of Semireduced and Oxidized Galactose Oxidase. Optical absorption spectra were recorded using a HP8453 or Cary 6000I spectrophotometer. Circular dichroism (CD) spectra were recorded on a Jasco J-710 spectropolarimeter using either a cylindrical cell or a masked 1 mL rectangular quartz cell (path length of 1 cm). Baseline adjustments were made by subtracting the buffer CD spectrum. X-Band EPR spectra were recorded on a Bruker EMX EPR spectrometer at 10 K using an Oxford cryostat. Semireduced enzyme samples (200 μL) in 100 mM potassium phosphate buffer (pH 7.0) in quartz EPR tubes were flash-frozen in liquid nitrogen prior to insertion into the cryostat. Spectral baseline correction was applied using WinEPR, and the spectra were simulated using SimFonia (Bruker).

Interactions with Azide. Oxidized or semireduced galactose oxidase was prepared as described above. After the optical and CD spectra of the enzyme had been recorded, sodium azide was added to a final concentration of 5 mM and the optical and CD spectra were recorded immediately. Azide dissociation constants were determined by titration of semireduced proteins with aliquots of freshly prepared 50 mM sodium azide in 50 mM potassium phosphate buffer (pH 7.0). Dissociation constants were determined from plots of $A_{obs} - A_o$ versus azide concentration via nonlinear curve fitting using a hyperbolic function (OriginLab), where A is the absorbance corresponding to the $N_3^- \rightarrow$ Cu(II) ligand-to-metal charge-transfer band occurring in the range of 370−383 nm. Solvent proton uptake by galactose oxidase upon azide binding was assessed via thymol blue-mediated titrations of the "as-purified" proteins at pH 8.0 (*43*, *44*). All solutions were CO_2-free. Galactose oxidase (80 μM) and thymol blue (80 μM) in 50 mM NaCl (final volume of 1 mL) were transferred to a 3 mL gastight cuvette containing a microstir bar (25 °C). Small aliquots (5−10 μL) of 1 mM NaOH were added until the change in absorbance at 600 nm became linear. The rate of uptake of protons was then measured by the change in absorbance at 600 nm after the addition of two aliquots of sodium azide. The concentration of azide added was based on the K_D for azide previously determined for each protein ($[N_3^-]$ added $= 10K_D$).

RESULTS

Biochemical Properties of the Mutational Variant Proteins. W290F, W290G, and W290H galactose oxidase were isolated in a pure form as determined by SDS−PAGE. Each W290 variant migrated as a single band with an anomalous electrophoretic mobility (apparent $M_r \sim 65$ kDa) similar to that of the mature wild-type galactose oxidase, and in contrast to the mobility expected for a protein identical in size to the wild-type protein but lacking the C228−Y272 thioether bond ($M_r \sim 68$ kDa) (*30*). Therefore, the SDS−PAGE results indicate that the thioether bond is completely formed in the W290 variants. Copper analysis of the wild type and W290 variant confirmed full copper loading: 1.2 ± 0.08 mol of Cu/mol of protein for the wild type, 0.96 ± 0.09 mol of Cu/mol of protein for W290F, 1.0 ± 0.06 mol of Cu/mol of protein for W290G, and 1.3 ± 0.1 mol of Cu/mol of protein for W290H. Wild-type and W290F galactose oxidase were oxidized to Cu(II)-Y$^\bullet$ by potassium ferricyanide ($E^{\circ\prime} = 424$ mV), whereas oxidation to W290H-Y$^\bullet$ and W290G-Y$^\bullet$ required cesium octacyanomolybdate ($E^{\circ\prime} = 892$ mV). Potassium ferrocyanide treatment was sufficient to reduce all the W290 variants to the Cu(II)-Y form.

Table 2: Kinetic Parameters for the Wild Type and W290 Variant Forms of Galactose Oxidase

	specific activity (units/mg)	K_m (mM)	k_{cat} (s^{-1})	k_{cat}/K_m (M^{-1} s^{-1})
		D-Galactose		
wild type	321 ± 6.7	82 ± 15.6	503 ± 16.2	6374 ± 709
W290F	96.6 ± 4.3	2950 ± 473.4	371 ± 43.0	129 ± 14
W290G	1.09 ± 0.04	1686 ± 457.3	1.66 ± 0.28	1.0 ± 0.2
W290H	0.445 ± 0.02	45 ± 4.5	0.24 ± 0.004	5.4 ± 0.3
		2-Methylene-1,3-propanediol		
wild type	221 ± 23	57 ± 4.1	283 ± 7.0	4965 ± 377
W290F	149 ± 6	29 ± 3.6	166 ± 6.4	5800 ± 763
W290G	0.005 ± 0.001	ND[a]	ND[a]	ND[a]
W290H	no measurable activity			

[a] Not determined.

Kinetic Properties. Using D-galactose as a substrate, the three W290 variants exhibited significantly lower specific activities (by factors of 3.3−720, Table 2) compared to that of wild-type galactose oxidase. The wild type and W290H exhibited saturation kinetics, with a k_{cat}/K_m for W290H 1000-fold lower than that of the wild type, whereas the activity of W290F and W290G exhibited an almost linear dependence on substrate concentration and could not be saturated with galactose. Values for k_{cat} and K_m could be reliably determined for only the wild type and W290H; approximate values were estimated for W290F and W290G obtained using the same data fitting method (Table 2).

Activities with 2-methylene-1,3-propanediol (2MP) were also examined. On the basis of modeling analysis, 2MP is unlikely to hydrogen bond to W290, as predicted for galactose binding (*39*, *46*), allowing the impact of this possible interaction to be assessed. Kinetic parameters are listed in Table 2. Note that turnover of 2MP by W290H could not be detected and that saturation kinetics were observed for only the wild-type enzyme and the W290F variant. It should be noted that the low activities of the W290G and W290H variants may be due, in part, to the difficulty of generating the tyrosyl radical under direct assay conditions, because of their elevated redox potentials.

Comparison of Crystal Structures of W290G, W290F, and the Wild Type−Azide Complex to Structures of the Wild Type and W290H. Crystallographic data for W290G, W290F, and the wild type−azide complex are listed in Table 1. All refined well, but the more limited resolution of W290F, and lower completeness for W290G, render these structures less accurate than the wild type−azide complex, W290H (*30*), and wild-type structures (*39*). Least-squares superposition of the

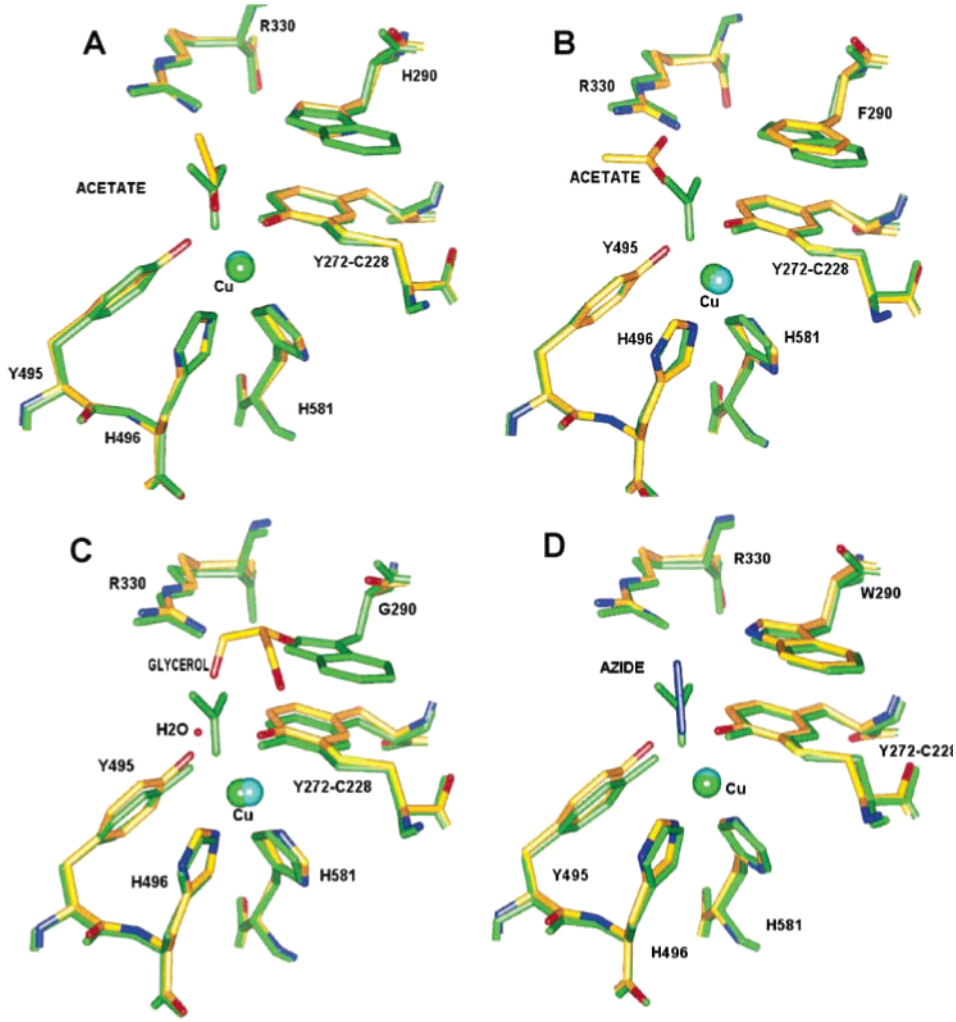

FIGURE 2: Active site of the W290 variants superimposed with wild-type galactose oxidase: (A) W290H, (B) W290F, (C) W290G, and (D) the wild type−azide complex. The structure of wild-type galactose oxidase is colored green, and that of the variant or azide structure is shown superimposed in atom-based color. The positions of the exogenous ligands in each structure are also shown. The figure was generated using SPOCK (*79*).

C_α atoms of W290G, W290F, and the azide complex with the wild-type structure (1GOF) give rms deviations of 0.37, 0.25, and 0.33 Å, respectively, showing the structures exhibit no significant overall changes. Notably, all the structures indicate that the thioether bond is fully formed and that copper is present at high occupancy, consistent with the SDS−PAGE and atomic absorption data reported above. As previously reported, the histidine ring in W290H superimposes well on the position of the five-membered ring of the tryptophan side chain (*30*). Additionally, the H290 ring nitrogen atom hydrogen bonds to the copper-bound acetate (2.92 Å, Figure 2A), suggesting the imidazole $N_\epsilon H$ group would be available for interaction with substrates, as proposed for the stacking tryptophan W290. H290 also occupies an alternative flipped (about χ_2) conformation in which N_ϵ points away and interacts with a water molecule. This result suggests that H290 displays greater mobility than W290. W290F lacks a ring NH group, which precludes hydrogen bonding to coordinated acetate. Acetate is observed in the W290F structure but interacts with R330 (Figure 2B). The phenyl ring of F290 shields the Y272−C228 radical site about as effectively as the indole ring of W290 and more completely than histidine. The absence of the side chain in the W290G variant permits a molecule of the cryoprotectant glycerol to bind, which partly occupies the position of the tryptophan side chain in the wild-type enzyme. The bound glycerol also encroaches on the site of the acetate ion, which has been replaced with a water molecule (Figure 2C). In the W290 variants, the axial tyrosine−copper distance is not significantly perturbed compared to the wild-type structure (Table 3) (*39*).

Table 3: Crystallographic Copper−Ligand Distances in Galactose Oxidase[a]

	temp (K)	Y272−Cu (Å)	Y495−Cu (Å)	exogenous ligand−Cu (Å, ligand)
wild type at pH 4.5	293	1.9	2.7	2.3, acetate
wild type at pH 7.0	293	1.9	2.6	2.8, water
W290H	293	1.8	2.5	2.7, acetate
W290F	100	2.1	2.7	4.1, acetate
W290G	100	2.1	2.8	3.2, water
wild type−azide complex	100	1.9	2.9	2.5, azide

[a] Errors in the coordination distances are difficult to estimate but are likely to be at least 0.1 Å for atoms in Y272 and Y495 and larger for water, azide, and acetate.

Replacement of W290 has implications for the solvent accessibility of the active site. In the wild-type enzyme, the

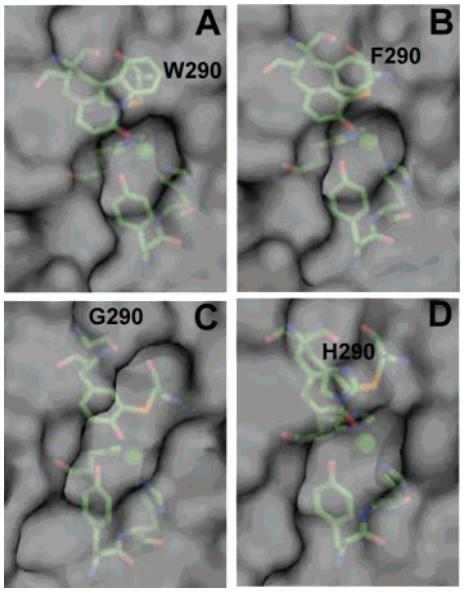

FIGURE 3: Solvent accessible contact surfaces of (A) the wild type, (B) W290F, (C) W290G, and (D) W290H. The copper ligands are shown with the solvent−protein contact surface represented in gray. Contact surface area for [C228−Y272] in the wild type (1GOF) is 1.69 Å^2, in W290F 2.02 Å^2, in W290G 9.28 Å^2, and in W290H 2.42 Å^2. The figure was produced using Pymol (DeLano Scientific).

radical site is protected from solvent by the hydrophobic indole side chain, and this is also true for W290F, since the phenyl ring is strongly hydrophobic and almost as large. In W290G, however, the absence of the side chain leaves Y272 exposed to solvent. This can be clearly seen in Figure 3, which shows a view of the solvent contact surfaces of the wild type and variants, looking into the active site from the solvent. While solvent accessibilities to the Y272−C228 cofactor in the wild type (Figure 3A) and W290F (Figure 3B) are broadly similar, W290G exhibits a dramatic opening of the cleft above the copper (Figure 3C), allowing solvent direct access to Y272, and this is where glycerol is observed to bind in the structure. H290 is calculated to shield the Y272−C228 cofactor (Figure 3D) more substantially than anticipated considering the instability of the W290H tyrosyl radical (vide infra).

In the wild type−azide complex (Figure 2D), N_3^- directly coordinates to the copper ion in bent, end-on geometry, with a copper-nitrogen distance of 2.5 Å and an angle of 121°, well within the range displayed by Cu(II)−N_3^- complexes of other copper-containing proteins. The terminal nitrogen atom of N_3^- hydrogen bonds (3.25 Å) to W290 $N_{\epsilon 1}$, which may influence binding of azide to the wild-type enzyme. Bond distances to the equatorial and axial tyrosines (Table 3) are consistent with an increase in the length of the Cu(II)−Y495 bond in the azide complex, as previously observed (*43*). Only small variations in the coordination geometry are evident in the various structures, and these are mostly below the significance level at the current resolution.

Stability of the Tyrosyl Radical. Rates for the Cu(II)-Y$^\bullet$ → Cu(II)-Y reaction in the W290 variant proteins varied widely (Table 4). At pH 7, W290F-Y$^\bullet$ had stability comparable ($k = 0.2$ h^{-1}) to that of the wild type ($k = 0.172$ h^{-1}), whereas W290G decayed more rapidly ($k = 2.72$ h^{-1}). The tyrosyl radical in W290H was the least stable, decaying rapidly at pH 7.0 ($k = 16.88$ h^{-1}).

Table 4: Tyrosyl Radical Decay Rates for Wild-Type Galactose Oxidase and W290 Variants

	decay rate (h^{-1})	
	phosphate buffer (pH 7.0)	acetate buffer (pH 4.5)
wild type	0.172 ± 0.0017	$3.95 \times 10^{-4} \pm 1.0 \times 10^{-4}$
W290F	0.20 ± 0.02	$1.06 \times 10^{-5} \pm 2.7 \times 10^{-4}$
W290G	2.72 ± 0.16	0.372 ± 0.13
W290H	16.88 ± 1.656	1.908 ± 0.216

While the kinetics of radical decay in the wild type, W290G, and W290H were monophasic (Figure 4 and Table 4), biphasic kinetics were observed for W290F (fast phase at 2.35 h^{-1}; slow phase at 0.2 h^{-1}). The decay rate of the second phase for W290F-Y$^\bullet$ is comparable to that of the wild type and represents 65% of the total absorbance change. The chemical nature of the initial fast phase has not yet been identified. Radical lifetimes were extended by rapid buffer exchange from pH 7.0 to 4.5. Although the tyrosyl radical in W290G and W290H is stabilized at pH 4.5, the decay is still faster than that of the wild type at pH 7.0. The W290F radical appears to be slightly more stable than wild-type galactose oxidase at pH 4.5. It should be noted that in addition to a pH shift, the acidic buffer also contains acetate that can bind to the copper ion.

Spectroscopy of Oxidized and Semireduced W290 Variants. As isolated, both the wild-type and W290F proteins display

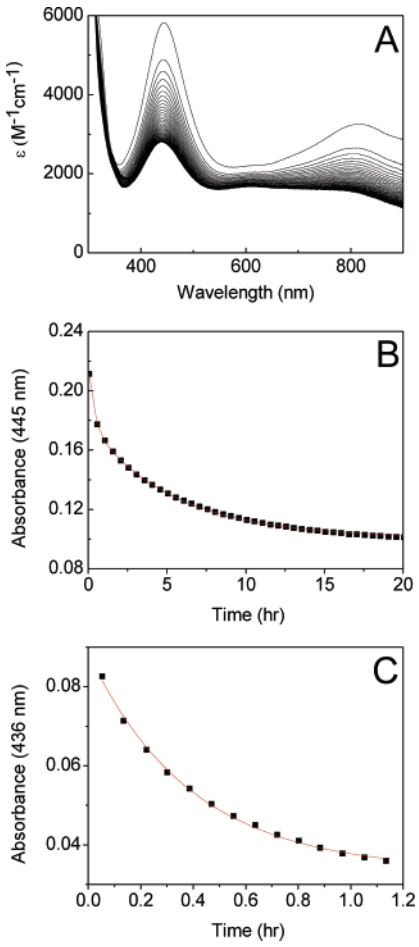

FIGURE 4: Optical spectra recorded at 30 min intervals showing (A) the decay of the tyrosyl radical in W290F in 100 mM potassium phosphate (pH 7.0) and (B) the change in A_{445} vs time. (C) Kinetics of tyrosyl radical decay in W290G in 100 mM potassium phosphate (pH 7.0).

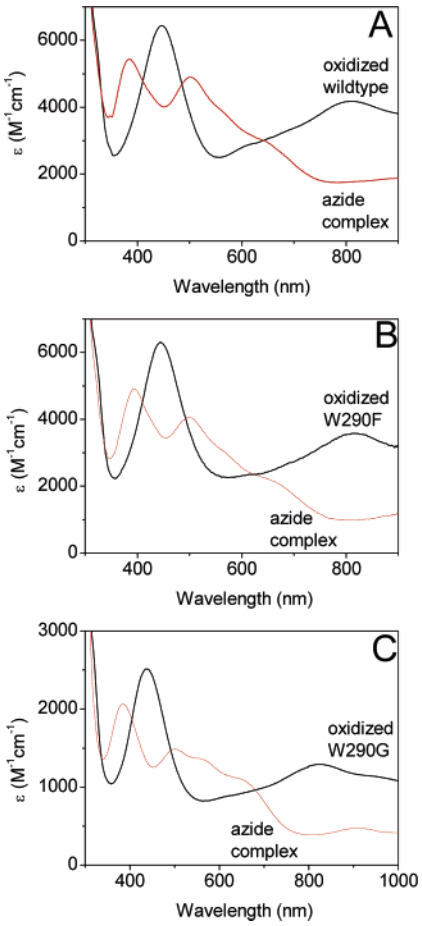

FIGURE 5: Optical spectra of oxidized galactose oxidase (black) and azide complexes (red) in 100 mM potassium phosphate (pH 7.0) for the wild type (A), W290F (B), and W290G (C).

thermochromic behavior (color changes from blue-green at 298 K to dusky pink at 193 K). In contrast, W290G and W290H were purple-pink and orange, respectively, at both temperatures. Note that as-isolated wild-type and W290F proteins are mixtures of the oxidized and semireduced states, whereas the W290G and W290H variants are probably in the semireduced state exclusively, because of their higher tyrosyl redox potentials.

Optical Spectra for the Oxidized Protein States. Wild-type Cu(II)-Y• has a distinctive electronic absorption spectrum, with two intense bands in the visible-near-infrared region: a peak at 445 nm attributed to overlapping phenolate → Cu(II) ligand-to-metal charge transfer (LMCT) and Y• $\pi \rightarrow \pi^*$ transitions and an intense low-energy transition at 810 nm, assigned as a ligand-to-ligand (LLCT) charge transfer transition (*60*), or a $\pi \rightarrow \pi^*$ transition of the radical (*61*). The optical spectra of the oxidized W290 variants are comparable to that of the wild-type enzyme (Figure 5 and Table 5). The spectra of W290F-Y• are most similar to that of the wild-type protein, whereas the energies of the characteristic electronic transitions are perturbed to a greater extent in W290G and W290H. Note that the smaller extinction coefficients of the W290G bands at 437 and 825 nm may be attributable, at least in part, to the lower stability of this variant. Given the rapid decay of oxidized W290H, only the band at ~455 nm could be reliably detected; Sykes and co-workers observed the transition at 828 nm in a transient kinetic experiment (*45*).

Optical and CD Spectra for the Semireduced Protein States. The electronic transitions of the semireduced enzymes are generally less intense than those associated with the radical copper site. Two bands are observed in the absorption spectrum of the wild-type enzyme at 441 nm [assigned as a phenolate → Cu(II) LMCT transition] and 630 nm (mixed copper ligand-field transition and LMCT) (*40*, *43*, *62*). Spectra of the W290 variants are generally similar (Figure 6) to those of the wild-type enzyme, especially the spectra of W290F. The exception is W290G, with the most prominent ligand-field absorption band observed at ~500 nm, reminiscent of the low-temperature or anion-bound forms of semireduced galactose oxidase (*63*, *64*).

As is frequently the case, the different selection rules for CD spectroscopy permit additional electronic transitions to be resolved (*65*). Remarkably, the CD spectra are more similar among the proteins than the absorption spectra, indicating that the electronic structure of the Cu(II) center is not grossly perturbed by second-coordination shell variations at W290. More specifically, the most prominent CD band at 625 nm has been assigned as a $^2B_1 \rightarrow {}^2B_2$ ($d_{x^2-y^2} \rightarrow d_{xy}$) transition, assuming effective C_{4v} symmetry for the Cu(II) complex (*43*, *66*). This assignment predicts additional ligand-field transitions to both higher and lower energy, which is consistent with the CD spectra. Note the positive CD feature in the semireduced spectra at ~314−325 nm, which is assigned as an N(π) imidazole → Cu(II) LMCT arising from the histidine ligands.

Inspection of Table 5 shows that the three Cu(II) ligand-field transitions (at 510, 625, and 785 nm in the wild type) vary in energy by approximately 670−790 cm^{-1} (or 4−5%) among the W290 proteins. Clearly, variation of the second coordination sphere at W290 produces a modest but measurable effect on the Cu(II) electronic structure. The properties of the azide complexes (see below) provide additional evidence for this effect.

EPR Spectroscopy. X-Band EPR spectra of the semireduced W290 variants at 10 K (data not shown) are closely similar, which is evident from the simulated $g_\perp$, $g_{||}$, and $A_{||}$ parameters presented in Table 6. The $g_\perp$, $g_{||}$, and $A_{||}$ values correspond to an axial type II copper center, in a tetragonal coordination geometry with a $d_{x^2-y^2}$ ground state (*67*). Except for a somewhat decreased $A_{||}$ seen for W290G, the parameters for the three W290 variants are closely similar to those obtained for the wild-type protein, indicating that the electronic ground state is not significantly affected by variations in the second coordination sphere at W290 at 10 K. Collectively, the electronic and magnetic data are consistent with a common first coordination sphere for Cu(II) in the four proteins and indicate that variations in the second coordination shell at W290 have a measurable, but relatively minor, impact on the electronic structure of the Cu(II) center. Variability in equatorial copper coordination (water, acetate, or no ligand) seen in the crystal structures (Figure 2) likely results from the different crystallographic buffer conditions that were used.

Azide Binding. Binding of azide to either oxidized or semireduced galactose oxidase generates an absorbance band at ~380 nm attributed to an N_3^- → Cu(II) LMCT band (Figures 5 and 6, summarized in Table 5). The energy and intensities of the N_3^- → Cu(II) LMCT transitions are consistent with equatorial coordination of the anion in all

Table 5: Comparison of Optical and CD Spectra of the Wild Type and W290 Variants of Galactose Oxidase

	Optical							
	wild type		W290F		W290G		W290H	
	λ (nm)	ϵ (M^{-1} cm^{-1})	λ (nm)	ϵ (M^{-1} cm^{-1})	λ (nm)	ϵ (M^{-1} cm^{-1})	λ (nm)	ϵ (M^{-1} cm^{-1})
Cu(II)-Y$^{\bullet}$	445	6436	445	6311	437	1290		
	810	4133	815	3582	825	2515		
Cu(II)-Y$^{\bullet}$−N_3^-	385	5437	394	4920	384	2062		
	500	4894	500	4054	500	1486		
			570	3993	567	1348		
	650	2945	665	2121	660	1070		
	900	1782			910	474		
Cu(II)-Y	441	887	430	1257	493	2029	480	1395
	630	1112	610	1425			630	914
Cu(II)-Y−N_3^-	380	2049	385	2396	370	3593	370	2239
	565	736	552	1035	510	1940	535	951
	775	539	745	352			720	397
	CD							
	λ (nm)	$\Delta\epsilon$ (M^{-1} cm^{-1})	λ (nm)	$\Delta\epsilon$ (M^{-1} cm^{-1})	λ (nm)	$\Delta\epsilon$ (M^{-1} cm^{-1})	λ (nm)	$\Delta\epsilon$ (M^{-1} cm^{-1})
Cu(II)-Y	314	4.79	325	1.62	320	1.85	318	2.23
	365	−0.14	358	−0.9	359	0.008		
	422	0.97	420	1.27	399	1.47	400	1.16
	510	0.42	515	0.42	497	0.83	495	0.73
	625	−2.89	625	−4.40	606	−3.47	600	−3.03
	785	0.69			745	1.44	752	2.12
Cu(II)-Y−N_3^-	320	0.87			335	0.027	355	0.006
	412	−1.48	404	−2.06	407	−0.78	395	−1.30
	555	−3.32	560	−3.14	511	−1.82	530	−1.67
					597	−1.42		
	750	1.56	740	1.24	722	0.83	720	1.03

cases, as observed in the crystal structure of the azide complex of the wild-type enzyme. Collectively, the shifts in the energy of the $N_3^- \rightarrow$ Cu(II) LMCT transition induced by the substitution at W290 are relatively minor, spanning ~600 cm^{-1} (~2% shift compared to that of the wild-type enzyme) in the oxidized complexes and ~700 cm^{-1} (~3%) in the semireduced complexes. Loss of the ~800 nm band in the azide complexes of the oxidized proteins may reflect protonation (and dissociation from copper) of Y495 induced by azide binding (Figure 5), as detailed previously (*43*). The band at 500 nm may be assigned, in part, as a $\pi \rightarrow \pi^*$ radical transition, indicative of the persistence of the tyrosyl radical in the W290 variants upon anion binding (*68*).

At first inspection, the CD spectra for the semireduced azide complexes are quite similar, with perturbations of the Cu(II) ligand-field bands on azide binding being comparable in magnitude. However, there is some variation in the energy and intensity of the CD bands (Figure 6 and Table 5). As anticipated, the CD for W290F·N_3^- is the most similar to that of the wild-type complex. The persistence of a weak negative CD feature around 597 nm ($\Delta\epsilon = -1.42$ M^{-1} cm^{-1}) in the spectrum of W290G·N_3^- suggests the presence of uncomplexed enzyme, consistent with the lower affinity of the variant for azide (vide infra). The shift of the 625 nm band to a higher energy in the wild-type enzyme has been interpreted as a change in copper geometry from square pyramidal to tetragonal initiated by the protonation and/or dissociation of the axial tyrosine ligand by either anion complexation, low pH, or low temperature (*64*). This shift of the ligand-field band to a higher energy is also evident in the spectra of the variants.

Cupric azide dissociation constants (K_D) were determined using semireduced protein in 50 mM potassium phosphate buffer (pH 7.0). The K_D values are as follows: 0.130 ± 0.006 mM for W290H < 0.146 ± 0.007 mM for the wild type < 0.730 ± 0.006 mM for W290F < 1.69 ± 0.057 mM for W290G. Clearly, variations in the second coordination sphere significantly perturb binding of azide to Cu(II), with the largest perturbation (W290G) resulting in an order of magnitude decrease in the affinity for the azide anion. Azide binding induces dissociation of the axial tyrosinate (Y495) and proton uptake. The H^+ uptake stoichiometries were as follows: 0.86 ± 0.003 proton/mol for the wild-type protein, in agreement with previous reports (*43*, *44*); 0.57 ± 0.01 proton/mol for W290H > 0.41 ± 0.009 proton/mol for W290F > 0.24 ± 0.006 proton/mol for W290G. According to the proposed mechanism of proton uptake (*63*), these data suggest that the pK_a of the axial tyrosine (Y495) has been perturbed significantly by side chain variation in the W290 position. This finding concurs with the previous assignment of a pK_a of 6.9 to the protonation of Y495 in the W290H variant, compared to a pK_a of 7.9 in the wild-type enzyme (*45*).

DISCUSSION

As discussed here, our data demonstrate that mutation of W290 in the second coordination shell of the copper active site in galactose oxidase produces substantial changes in some enzyme characteristics (radical stability and kinetic parameters) while only slightly perturbing others (geometry and ground-state electronic structure). Structural, spectroscopic, and kinetic analyses establish that the predominant factors are likely to be the altered solvent accessibility of the [Cu(II)-Y$^{\bullet}$] site, although subtle second-shell electronic effects may also contribute to modulating reactivity. An additional effect is that loss of the W290 ring NH group apparently decreases the affinity for D-galactose.

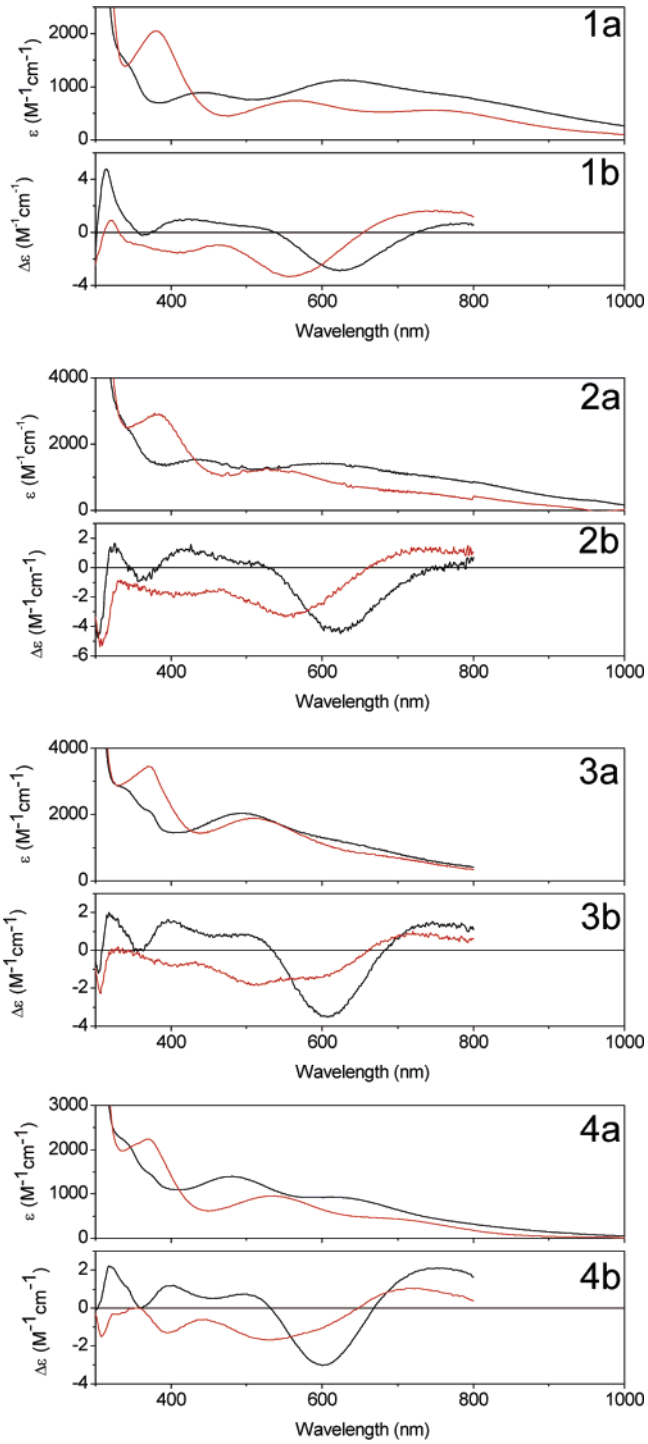

FIGURE 6: Optical (a) and CD (b) spectra of semireduced galactose oxidase (black) and azide complexes (red) in 100 mM potassium phosphate (pH 7.0) for the wild type (1), W290F (2), W290G (3), and W290H (4).

Table 6: X-Band EPR Simulation Parameters for the Wild Type and W290 Variants of Galactose Oxidase at 10 K

	$g_{\|\|}$	$g_{\perp}$	$A_{\|\|}$ (MHz)	⊥ line width (G)	|| line width (G)
wild type	2.274	2.0570	518	60	50
W290F	2.270	2.0565	510	58	40
W290G	2.274	2.0570	488	60	50
W290H	2.274	2.0574	518	58	50

Structural Characteristics and Active Site Biochemical Properties of the Mutational Variants. There are no substantial changes in structure between the the wild type and W290X variants (Figure 2), apart from the change in residue at position 290. The crystal structures also established unambiguously that the thioether bond in the C228−Y272 cofactor is present in all the variants, substantiating the SDS−PAGE analysis (*30*). A key structural change during processing of the precursor protein is a 6.3 Å movement of the W290 C_{α} atom that moves this residue into its stacking location over the thioether bond (*69*). Our data clearly show that the side chain of W290 is not absolutely required for this structural reorganization. Apparently, the indole side chain of W290 is not obligatory for the processing steps leading to thioether bond formation, although further study would be needed to establish whether the rates of these processing steps are affected. Furthermore, the copper analysis results establish that W290 is not essential for metal incorporation. The results from copper analysis were supported by the protein crystallography, which revealed strong electron density at the metal site in all variants. Consequently, altered catalytic properties of the W290 variants compared to those of the wild-type enzyme are not due to substoichiometric copper incorporation or incomplete processing.

However, the resolution of the structures, especially for W290F and W290G, does not allow evaluation of perturbations in the bonding and electronic structure, such as electronic coupling between Cu(II) and the singly occupied orbital on $Y^{\bullet}$, which requires a higher degree of accuracy. Spectroscopic data are more informative in this regard.

Tyrosyl Radical Generation and Stability. Previous work (*45*) has established the redox potential for the [Cu(II)-$Y^{\bullet}$]/[Cu(II)-Y] couple to be ~730 mV for W290H. We observed that a strong oxidant, cesium octacyanomolybdate ($E^{\circ\prime}$ = 892 mV), is required for generation of the activated states of W290G (and W290H), whereas a weaker oxidant, potassium ferricyanide ($E^{\circ\prime}$ = 424 mV), was sufficient to oxidize the wild-type and W290F proteins. Remarkably, substitution of H or G at W290 has a larger effect on the cofactor tyrosine (Y272) redox potential than does removal of the coordinating copper, which increases the redox potential to only 570 mV (*70*). Thus, it appears that hydrophobic aromatic residues lead to lower redox potentials whereas smaller polar residues or the absence of a side chain leads to higher redox potentials. These results indicate that W290 plays a significant role in controlling the redox potential of the free radical site. Model systems (*71*) had not revealed this effect, which is clearly dependent on the chemical nature of the stacking residue at position 290.

The stabilities of the radical site in the wild type and W290F are comparable at pH 7, and the decay rates are a factor of 10−1000-fold slower than for W290G and W290H, suggesting that a hydrophobic residue at position 290 increases radical stability and lowers $E^{\circ\prime}$. EPR experiments (*14*, *67*, *72*, *73*) indicate that spin density is not delocalized over W290 in the wild-type enzyme, but this does not preclude an electronic stabilizing effect from a stacking aromatic ring (*74*). It is reasonable to suppose that a radical site exposed to solvent (e.g., the W290G variant) would be less stable than a site protected by a hydrophobic, aromatic "lid". Solvent contact surface representations show that Y272 in the W290F and W290H variants appears slightly more exposed than in the wild type and that W290G provides little protection for the radical (Figure 3). The unexpectedly low

solvent contact surface area to the C228−Y272 cofactor calculated for W290H (2.42 Å^2) does not appear to correlate with the highly unstable character of the tyrosyl radical in this variant, which is less stable than the tyrosyl radical in W290G. However, H290 apparently occupies two conformations in the crystal structure, consistent with increased side chain mobility; together with its increased polarity and H-bonding capability, these characteristics of H290 may enhance solvent accessibility, which could partly account for the accelerated decay of W290H-Y•. Alternatively, instability of the tyrosyl radical in W290H may reflect enhancement of specific radical decay pathways by the imidazole ring.

It is striking that the stability of the radical site in the wild type and W290F increases dramatically (3−4 orders of magnitude) when the pH is lowered from 7.0 to 4.5 (Table 4). At pH 4.5, the red absorption band (at 810 nm) of oxidized galactose oxidase is lost, possibly resulting from dissociation of Y495 from the copper ion (*13*, *29*). Enhanced radical stability at pH 4.5 may result from disruption of an electronic interaction between Y495 and Y272•, mediated by Cu(II), perhaps by abolishing a radical decay pathway via Y495. Notably, the radical in both W290G and W290H also displays increased stability at pH 4.5, but by approximately 1 order of magnitude. This attenuated difference in stability may reflect partial dissociation of Y495 at neutral pH for the latter variants (vide infra). At pH 4.5, the exogenous copper ligand is acetate from the buffer, and we cannot fully discount the possibility that this may also contribute to the increased stability of the radical at this pH despite the observation that addition of acetate at pH 7.0 did not improve the stability of the radical in the W290H variant.

Sequence alignments suggest that the stacking tryptophan of galactose oxidase may be replaced with histidine in glyoxal oxidase. While the degree of sequence similarity is less than 20%, the key active site residues are conserved (*13*). The glyoxal oxidase radical has a redox potential of 0.64 V (galactose oxidase, 0.43 V) (*41*) and is 43-fold less stable than the galactose oxidase radical (*13*, *75*). These differences between galactose oxidase and glyoxal oxidase further illustrate the modulating effects of the residue stacked over [C228−Y272•].

Kinetic Properties. Immediately evident from Table 2 is the fact that substitution at W290 has substantial effects on galactose oxidase catalysis. Although the catalytic ability of the W290F variant is reduced, it is clearly the most competent catalyst among the variants, whereas W290G and W290H are severely compromised. Further, the K_m for D-galactose in W290F is strikingly elevated (>1000 mM) compared to that of the wild type (82 mM), implying a role for W290 in binding D-galactose, probably by hydrogen bonding. Indirect evidence of the role of W290 in substrate binding may be inferred by a hydrogen bond between W290 and the acetate copper ligand (2.84 Å from W290 $N_{\epsilon 1}$ to acetate O; 1GOF). In contrast, the acetate nearest the copper ion in the W290F crystal structure is 4.08 Å away and is hydrogen bonded to R330. A closer correspondence in K_m values for 2-methylene-1,3-propanediol as a substrate, where such H-bonding to W290 is not possible, supports this inference. Model building studies (*39*, *46*, *76*) have also predicted a H-bonding interaction between W290 and D-galactose. The value of k_{cat} for W290F (371 s^{-1}) is comparable in magnitude to that of the wild type (503 s^{-1}), reinforcing the conclusion that W290F can be a competent catalyst when the substrate concentration is high.

Although the specific activity of W290H with D-galactose as a substrate is very low, the K_m (45 mM) is more favorable than that of the wild type. The observation of a H-bond between H290 and coordinated acetate (2.92 Å, similar to that observed for the wild-type enzyme) supports the hypothesis that H-bonding from position 290 is important to D-galactose binding. The low specific activity in W290H may be attributed to the protein being predominantly in the enzymatically inactive semireduced state. Although the presence of peroxidase in the coupled assay (see Experimental Procedures) is sufficient to support oxidization of the wild-type enzyme and W290F, the elevated redox potential of the free radical site in W290H precludes this. Note that the value of K_m determined for W290H is an accurate estimate since, unlike k_{cat}, it does not require that the enzyme be fully activated. W290G also displays a low specific activity that may be attributed to the high redox potential required to activate this site.

Spectroscopic Studies of the W290 Variants. Thermochromic behavior of wild-type galactose oxidase has been modeled as an equilibrium involving the transfer of a proton from Cu(II)-H_2O to Y495, leading to dissociation of Y495 from copper at low temperatures (*63*). Investigation of the thermochromic properties of the as-isolated W290 variants (largely in the semireduced state) suggests that the axial ligand Y495 is coordinated to copper in W290F at 298 K, whereas Y495 is mostly dissociated from copper in W290G and W290H. Such an outcome is relevant to the interpretation of the spectroscopic results and the proton uptake results discussed below. Note that for crystal structures based on data collected at 100 K, the Cu(II)−Y495 O distance is anticipated to reflect at least partial dissociation.

The spectroscopic data establish that the perturbations of the electronic structure of the galactose oxidase active site, induced by side chain variation at position 290, are relatively modest, in both the semireduced state and the catalytically important oxidized state. The EPR spectra for the semireduced forms of the wild type and W290 variants are essentially identical and indicate that there are no major differences in the geometry of the copper centers at 10 K. At this temperature, Y495 is expected to be completely dissociated for all samples such that the EPR parameters reflect only equatorial bonding and a tetragonal geometry, which must then be essentially identical for the wild-type enzyme and the W290 variants.

Interactions with Azide. Azide coordination mimics the binding behavior of galactose oxidase substrates (*42*, *43*) and thus serves as a model for this reaction. The crystal structure of the azide complex (Figure 2D) establishes that the ligand coordinates in an equatorial position, with the expected bent, end-on geometry, and that Y495 has moved to a greater distance from the copper. The terminal nitrogen atom of the azide anion is hydrogen bonded to W290, further suggesting a role for the residue in substrate binding. Electronic spectra of the azide complexes, for both the semireduced and oxidized states, of the wild type and W290 variants confirm equatorial azide coordination. In the oxidized complex, the absence of the red band at ~810 nm would be consistent with protonation of Y495 and its dissociation from copper.

Despite the close similarities in the electronic structures of the azide complexes of the wild-type enzyme and the W290 variants, the K_{eq} for binding of azide to Cu(II) in the semireduced forms of the proteins is substantially altered by the conservative variations in the second coordination sphere. Once again, the most straightforward interpretation of this effect is that mutation of the residue at position 290 alters properties of the active site microenvironment, e.g., solvent accessibility and polarity, which perturbs the thermodynamics for azide binding.

CONCLUSIONS

The data presented herein demonstrate that, for a series of structurally characterized derivatives, conservative mutations of a single second-coordination shell residue can produce significant changes in critical aspects of active site reactivity. Such a result is hardly surprising, but the particular mechanisms that modulate the reactivity of the Cu(II) radical site in galactose oxidase are interesting and illustrative. Most obviously, the dramatic increase in the K_m for D-galactose in W290F is strong evidence that W290 is involved in recognition and binding of some substrates. It can be argued that the relatively similar magnitudes for the K_m for D-galactose in the wild type and W290H (as compared to the other variants) indicate that hydrogen bonding, at least for D-galactose, between substrates and W290 is important. W290 is one of several residues in the active site of galactose oxidase that can hydrogen bond to sugar substrates, and the totality of these hydrogen bonding interactions govern the stereospecificity of the enzyme (*46*, *49*, *77*, *78*).

The detailed comparisons among the W290 mutational variants and the wild-type enzyme (see also ref *45*) provide compelling evidence that W290 plays an important role in lowering the redox potential from that normally required for generation of tyrosine radical at Y272. Moreover, W290 clearly contributes to the stability of the active site tyrosine radical; it is likely that both electronic and steric effects associated with the stacking of the indole ring with the cross-linked tyrosine−cysteine cofactor contribute. W290 may also modulate the reactivity of Y495, which has been implicated to function as the active site base in turnover. This effect may be a consequence of the role of W290 in the active site microenvironment and may also be evident in the impact of mutational variations at position 290 on the thermodynamics of binding of azide to Cu(II). These findings have potentially important implications for modeling and theoretical studies of the galactose oxidase active site: perturbations of weak interactions modulated by W290 have substantial impacts on reactivity without having major perturbations on the electronic structure and bonding of the Cu(II) and its ligands.

Finally, W290F has characteristics comparable to those of the wild type with respect to radical generation and stability but is much less competent with regard to D-galactose recognition and binding. W290H displays D-galactose affinity similar to that of the wild-type enzyme, while lacking the thermodynamic and kinetic stabilization of the radical. Therefore, the choice of tryptophan at position 290 may best satisfy necessary reactivity constraints. It is not surprising that mutations to W290 are pleiotropic, since the active site of the enzyme is a delicately poised and optimized environment, and changing any one of amino acids in the active site would affect this balance.

ACKNOWLEDGMENT

We thank Mark R. Parsons for assistance with processing of the crystallographic data for the W290F variant. We are also grateful for facilities provided by the BBSRC-funded North of England Structural Biology Centre (NESBIC).

REFERENCES

1. Stubbe, J. A. (1989) Protein radical involvement in biological catalysis, *Annu. Rev. Biochem. 58*, 257−285.
2. Stubbe, J., and van der Donk, W. A. (1998) Protein radicals in enzyme catalysis, *Chem. Rev. 98*, 705−762.
3. Frey, P. A. (2001) Radical mechanisms of enzymatic catalysis, *Annu. Rev. Biochem. 70*, 121−148.
4. Reichard, P., and Ehrenberg, A. (1983) Ribonucleotide reductase: A radical enzyme, *Science 221*, 514−519.
5. Eklund, H., Uhlin, U., Farnegardh, M., Logan, D. T., and Nordlund, P. (2001) Structure and function of the radical enzyme ribonucleotide reductase, *Prog. Biophys. Mol. Biol. 77*, 177−268.
6. Stubbe, J., Nocera, D. G., Yee, C. S., and Chang, M. C. (2003) Radical initiation in the class I ribonucleotide reductase: Long-range proton-coupled electron transfer? *Chem. Rev. 103*, 2167−2201.
7. Kolberg, M., Logan, D. T., Bleifuss, G., Potsch, S., Sjoberg, B. M., Graslund, A., Lubitz, W., Lassmann, G., and Lendzian, F. (2005) A new tyrosyl radical on Phe208 as ligand to the diiron center in *Escherichia coli* ribonucleotide reductase, mutant R2-Y122H, Combined X-ray diffraction and EPR/ENDOR studies, *J. Biol. Chem. 280*, 11233−11246.
8. Sancar, A. (2003) Structure and function of DNA photolyase and cryptochrome blue-light photoreceptors, *Chem. Rev. 103*, 2203−2237.
9. Sivaraja, M., Goodin, D. B., Smith, M., and Hoffman, B. M. (1989) Identification by ENDOR of Trp191 as the free-radical site in cytochrome *c* peroxidase compound ES, *Science 245*, 738−740.
10. Knappe, J., and Wagner, A. F. (2001) Stable glycyl radical from pyruvate formate-lyase and ribonucleotide reductase(III), *Adv. Protein Chem. 58*, 277−315.
11. Ballinger, M. D., Reed, G. H., and Frey, P. A. (1992) An organic radical in the lysine 2,3-aminomutase reaction, *Biochemistry 31*, 949−953.
12. Tsai, A., and Kulmacz, R. J. (2000) Tyrosyl radicals in prostaglandin H synthase-1 and -2, *Prostaglandins Other Lipid Mediators 62*, 231−254.
13. Whittaker, M. M., Kersten, P. J., Nakamura, N., Sanders-Loehr, J., Schweizer, E. S., and Whittaker, J. W. (1996) Glyoxal oxidase from *Phanerochaete chrysosporium* is a new radical-copper oxidase, *J. Biol. Chem. 271*, 681−687.
14. Whittaker, M. M., and Whittaker, J. W. (1990) A tyrosine-derived free radical in apogalactose oxidase, *J. Biol. Chem. 265*, 9610−9613.
15. Kim, S. Y., and Barry, B. A. (1998) The protein environment surrounding tyrosyl radicals $D^{\bullet}$ and $Z^{\bullet}$ in photosystem II: A difference Fourier-transform infrared spectroscopic study, *Biophys. J. 74*, 2588−2600.
16. Narvaez, A. J., Kalman, L., LoBrutto, R., Allen, J. P., and Williams, J. C. (2002) Influence of the protein environment on the properties of a tyrosyl radical in reaction centers from *Rhodobacter sphaeroides*, *Biochemistry 41*, 15253−15258.
17. Barrows, T. P., Bhaskar, B., and Poulos, T. L. (2004) Electrostatic control of the tryptophan radical in cytochrome *c* peroxidase, *Biochemistry 43*, 8826−8834.
18. Perez-Boada, M., Ruiz-Duenas, F. J., Pogni, R., Basosi, R., Choinowski, T., Martinez, M. J., Piontek, K., and Martinez, A. T. (2005) Versatile peroxidase oxidation of high redox potential aromatic compounds: Site-directed mutagenesis, spectroscopic and crystallographic investigation of three long-range electron transfer pathways, *J. Mol. Biol. 354*, 385−402.
19. Gerez, C., Elleingand, E., Kauppi, B., Eklund, H., and Fontecave, M. (1997) Reactivity of the tyrosyl radical of *Escherichia coli* ribonucleotide reductase: Control by the protein, *Eur. J. Biochem. 249*, 401−407.

20. Ormo, M., Regnstrom, K., Wang, Z., Que, L., Jr., Sahlin, M., and Sjoberg, B. M. (1995) Residues important for radical stability in ribonucleotide reductase from *Escherichia coli*, *J. Biol. Chem. 270*, 6570−6576.
21. Zhang, J., Zheng, H., Groce, S. L., and Lipscomb, J. D. (2006) Basis for specificity in methane monooxygenase and related non-heme iron-containing biological oxidation catalysts, *J. Mol. Catal. A: Chem. 251*, 54−65.
22. Kohzuma, T., Inoue, T., Yoshizaki, F., Sasakawa, Y., Onodera, K., Nagatomo, S., Kitagawa, T., Uzawa, S., Isobe, Y., Sugimura, Y., Gotowda, M., and Kai, Y. (1999) The structure and unusual pH dependence of plastocyanin from the fern *Dryopteris crassirhizoma*. The protonation of an active site histidine is hindered by $\pi-\pi$ interactions, *J. Biol. Chem. 274*, 11817−11823.
23. Chen, K., Tilley, G. J., Sridhar, V., Prasad, G. S., Stout, C. D., Armstrong, F. A., and Burgess, B. K. (1999) Alteration of the reduction potential of the $[4Fe\text{-}4S]^{2+/+}$ cluster of *Azotobacter vinelandii* ferredoxin I, *J. Biol. Chem. 274*, 36479−36487.
24. Xie, J., Yikilmaz, E., Miller, A. F., and Brunold, T. C. (2002) Second-sphere contributions to substrate-analogue binding in iron(III) superoxide dismutase, *J. Am. Chem. Soc. 124*, 3769−3774.
25. Zoidakis, J., Sam, M., Volner, A., Han, A., Vu, K., and Abu-Omar, M. M. (2004) Role of the second coordination sphere residue tyrosine 179 in substrate affinity and catalytic activity of phenylalanine hydroxylase, *J. Biol. Inorg. Chem. 9*, 289−296.
26. Miranda, F. F., Kolberg, M., Andersson, K. K., Geraldes, C. F., and Martinez, A. (2005) The active site residue tyrosine 325 influences iron binding and coupling efficiency in human phenylalanine hydroxylase, *J. Inorg. Biochem. 99*, 1320−1328.
27. Tomchick, D. R., Phan, P., Cymborowski, M., Minor, W., and Holman, T. R. (2001) Structural and functional characterization of second-coordination sphere mutants of soybean lipoxygenase-1, *Biochemistry 40*, 7509−7517.
28. Borovik, A. S. (2005) Bioinspired hydrogen bond motifs in ligand design: The role of noncovalent interactions in metal ion mediated activation of dioxygen, *Acc. Chem. Res. 38*, 54−61.
29. Rogers, M. S., Knowles, P. F., Baron, A. J., McPherson, M. J., and Dooley, D. M. (1998) Characterization of the active site of galactose oxidase and its active site mutational variants Y495F/H/K and W290H by circular dichroism spectroscopy, *Inorg. Chim. Acta 275*−*276*, 175−181.
30. Baron, A. J., Stevens, C., Wilmot, C., Seneviratne, K. D., Blakeley, V., Dooley, D. M., Phillips, S. E. V., Knowles, P. F., and McPherson, M. J. (1994) Structure and mechanism of galactose oxidase. The free radical site, *J. Biol. Chem. 269*, 25095−25105.
31. Ito, N., Phillips, S. E., Stevens, C., Ogel, Z. B., McPherson, M. J., Keen, J. N., Yadav, K. D., and Knowles, P. F. (1991) Novel thioether bond revealed by a 1.7 Å crystal structure of galactose oxidase, *Nature 350*, 87−90.
32. Okeley, N. M., and van der Donk, W. A. (2000) Novel cofactors via post-translational modifications of enzyme active sites, *Chem. Biol. 7*, 159−171.
33. Amaral, D., Bernstein, L., Morse, D., and Horecker, B. L. (1963) Galactose oxidase of *Polyporus circinatus*: A copper enzyme, *J. Biol. Chem. 238*, 2281−2284.
34. Sun, L., Petrounia, I. P., Yagasaki, M., Bandara, G., and Arnold, F. H. (2001) Expression and stabilization of galactose oxidase in *Escherichia coli* by directed evolution, *Protein Eng. 14*, 699−704.
35. Kosman, D. J. (1984) Galactose Oxidase, in *Copper Proteins and Copper Enzymes* (Lontie, R., Ed.) pp 1−26, CRC Press, Boca Raton, FL.
36. Avigad, G., Amaral, D., Asensio, C., and Horecker, B. L. (1962) The D-galactose oxidase of *Polyporus circinatus*, *J. Biol. Chem. 237*, 2736−2743.
37. Silakowski, B., Ehret, H., and Schairer, H. U. (1998) fbfB, a gene encoding a putative galactose oxidase, is involved in *Stigmatella aurantiaca* fruiting body formation, *J. Bacteriol. 180*, 1241−1247.
38. Leuthner, B., Aichinger, C., Oehmen, E., Koopmann, E., Muller, O., Muller, P., Kahmann, R., Bolker, M., and Schreier, P. H. (2005) A H_2O_2-producing glyoxal oxidase is required for filamentous growth and pathogenicity in *Ustilago maydis*, *Mol. Genet. Genomics 272*, 639−650.
39. Ito, N., Phillips, S. E. V., Yadav, K. D. S., and Knowles, P. F. (1994) Crystal structure of a free radical enzyme, galactose oxidase, *J. Mol. Biol. 238*, 794−814.
40. Whittaker, M. M., and Whittaker, J. W. (1988) The active site of galactose oxidase, *J. Biol. Chem. 263*, 6074−6080.
41. Johnson, J. M., Halsall, H. B., and Heineman, W. R. (1985) Redox activation of galactose oxidase: Thin-layer electrochemical study, *Biochemistry 24*, 1579−1585.
42. Knowles, P. F., Brown, R. D., Koenig, S. H., Wang, S., Scott, R. A., McGuirl, M. A., Brown, D. E., and Dooley, D. M. (1995) Spectroscopic studies of the active site of galactose oxidase, *Inorg. Chem. 34*, 3895−3902.
43. Whittaker, M. M., and Whittaker, J. W. (1993) Ligand interactions with galactose oxidase: Mechanistic insights, *Biophys. J. 64*, 762−772.
44. Reynolds, M. P., Baron, A. J., Wilmot, C. W., Vinecombe, E., Stevens, C., Phillips, S. E. V., Knowles, P. F., and McPherson, M. J. (1997) Structure and mechanism of galactose oxidase: Catalytic role of tyrosine 495, *J. Biol. Inorg. Chem. 2*, 327−335.
45. Saysell, C. G., Barna, T., Borman, C. D., Baron, A. J., McPherson, M. J., and Sykes, A. G. (1997) Properties of the Trp290His variant of *Fusarium* NRRL 2903 galactose oxidase: Interactions of the $GOase_{semi}$ state with different buffers, its redox activity and ability to bind azide, *J. Biol. Inorg. Chem. 2*, 702−709.
46. Wachter, R. M., and Branchaud, B. P. (1996) Molecular modeling studies on oxidation of hexopyranoses by galactose oxidase. An active site topology apparently designed to catalyze radical reactions, either concerted or stepwise, *J. Am. Chem. Soc. 118*, 2782−2789.
47. Whittaker, M. M., Duncan, W. R., and Whittaker, J. W. (1996) Synthesis, structure and properties of a model for galactose oxidase, *Inorg. Chem. 35*, 382−386.
48. McPherson, M. J., Parsons, M. R., Spooner, R. K., and Wilmot, C. M. (2001) Galactose Oxidase, in *Handbook of Metalloproteins* (Wieghart, K., Poulas, T. L., Huber, R., and Messerschmidt, A., Eds.) Vol 2, pp 1245−1257, Wiley, New York.
49. Deacon, S. E., Mahmoud, K., Spooner, R. K., Firbank, S. J., Knowles, P. F., Phillips, S. E., and McPherson, M. J. (2004) Enhanced fructose oxidase activity in a galactose oxidase variant, *ChemBioChem 5*, 972−979.
50. Kosman, D. J., Ettinger, M. J., Weiner, R. E., and Massaro, E. J. (1974) The molecular properties of the copper enzyme galactose oxidase, *Arch. Biochem. Biophys. 165*, 456−467.
51. Leslie, A. G. W. (1992) *Joint CCP4+ESF-EAMCB Newsletter on Protein, Cyrstallography*, Vol. 26, Daresbury Laboratory, Warrington, U.K.
52. Collaborative Computational Project Number 4 (1994) *Acta Crystallogr. D50*, 760−763.
53. Firbank, S. J. (2002) Structural investigation of processing and catalysis in galactose oxidase, Ph.D. Thesis, University of Leeds, Leeds, U.K.
54. Otwinowski, Z., and Minor, W. (1997) Processing of X-ray diffraction data collected in oscillation mode, *Methods Enzymol. 276*, 307−326.
55. Vinecombe, E. (1999) X-ray crystallographic studies on copper-containing oxidases, Ph.D. Thesis, University of Leeds, Leeds, U.K.
56. Kleywegt, G. J., and Jones, T. A. (1994) *CCP4/ESF-EACBM Newsletter on Protein Crystallography 31*, 9−14.
57. Lee, B., and Richards, F. M. (1971) The interpretation of protein structures: Estimation of static accessibility, *J. Mol. Biol. 55*, 379−400.
58. Hawkridge, F. M., and Kuwana, T. (1973) Indirect coulometric titration of biological electron transport components, *Anal. Chem. 45*, 1021−1026.
59. Kolthoff, I. M., and Tomsicek, W. J. (1936) The oxidation potential of the system potassium molybdocyanide-molybdocyanide and the effect of neutral salts on the potential, *J. Phys. Chem. 40*, 247−255.
60. McGlashen, M. L., Eads, D. D., Spiro, T. G., and Whittaker, J. W. (1995) Resonance raman spectroscopy of galactose oxidase: A new interpretation based on model compound free radical spectra, *J. Phys. Chem. 99*, 4918−4922.
61. Rokhsana, D., Dooley, D. M., and Szilagyi, R. K. (2006) Structure of the oxidized active site of galactose oxidase from realistic in silico models, *J. Am. Chem. Soc. 128*, 15550−15551.
62. Whittaker, J. W. (1995) Spectroscopic studies of galactose oxidase, in *Redox-active Amino Acids in Biology* (Klinman, J. P., Ed.) pp 262−278, Academic Press, San Diego.
63. Whittaker, M. M., Ekberg, C. A., Peterson, J., Sendova, M. S., Day, E. P., and Whittaker, J. W. (2000) Spectroscopic and magnetochemical studies on the active site copper complex in galactose oxidase, *J. Mol. Catal. B: Enzym. 8*, 3−15.

64. Whittaker, J. W. (2002) Galactose oxidase, *Adv. Protein Chem. 60*, 1−49.
65. Johnson, M. K. (2001) CD and MCD Spectrocopy in *Physical Methods in Bioinorganic Chemistry: Spectroscopy and Magnetism*, (Que, L., Ed.) University Science Books, Sausalito, CA.
66. Whittaker, J. W. (1994) The free radical-coupled copper active site of galactose oxidase, in *Metalloenzymes involving amino acid residues and related radicals* (Sigel, H., and Sigel, A., Eds.) Marcel Dekker, New York.
67. Peisach, J., and Blumberg, W. E. (1974) Structural implications derived from the analysis of electron paramagnetic resonance spectra of natural and artificial copper proteins, *Arch. Biochem. Biophys. 165*, 691−708.
68. Whittaker, M. M., DeVito, V. L., Asher, S. A., and Whittaker, J. W. (1989) Resonance Raman evidence for tyrosine involvement in the radical site of galactose oxidase, *J. Biol. Chem. 264*, 7104−7106.
69. Firbank, S. J., Rogers, M. S., Wilmot, C. M., Dooley, D. M., Halcrow, M. A., Knowles, P. F., McPherson, M. J., and Phillips, S. E. V. (2001) Crystal structure of the precursor of galactose oxidase: An unusual self-processing enzyme, *Proc. Natl. Acad. Sci. U.S.A. 98*, 12932−12937.
70. Wright, C., and Sykes, A. G. (2001) Interconversion of Cu^{I} and Cu^{II} forms of galactose oxidase: Comparison of reduction potentials, *J. Inorg. Biochem. 85*, 237−243.
71. Halcrow, M. A. (2002) Dissecting an enzyme: Model compounds for the galactose oxidase radical site, *Heteroat. Chem. 13*, 494−500.
72. Gerfen, G. J., Bellew, B. F., Griffin, R. G., Singel, D. J., Ekberg, C. A., and Whittaker, J. W. (1996) High-frequency electron paramagnetic resonance spectroscopy of the apogalactose oxidase radical, *J. Phys. Chem. 100*, 16739−16748.
73. Babcock, G. T., El-Deeb, M. K., Sandusky, P. O., Whittaker, M. M., and Whittaker, J. W. (1992) Electron paramagnetic resonance and electron nuclear double resonance spectroscopies of the radical site in galactose oxidase and of thioether-substituted phenol model compounds, *J. Am. Chem. Soc. 114*, 3727−3734.
74. Rogers, M. S., and Dooley, D. M. (2001) Posttranslationally modified tyrosines from galactose oxidase and cytochrome *c* oxidase, *Adv. Protein Chem. 58*, 387−436.
75. Whittaker, M. M., Ballou, D. P., and Whittaker, J. W. (1998) Kinetic isotope effects as probes of the mechanism of galactose oxidase, *Biochemistry 37*, 8426−8436.
76. Whittaker, J. W. (2005) The radical chemistry of galactose oxidase, *Arch. Biochem. Biophys. 433*, 227−239.
77. Ito, N., Philips, S. E., Stevens, C., Ogel, Z. B., McPherson, M. J., Keen, J. N., Yadav, K. D., and Knowles, P. F. (1992) Three-dimensional structure of galactose oxidase: An enzyme with a built-in secondary cofactor, *Faraday Discuss. 93*, 75−84.
78. Sun, L., Bulter, T., Alcalde, M., Petrounia, I. P., and Arnold, F. H. (2002) Modification of galactose oxidase to introduce glucose 6-oxidase activity, *ChemBioChem*, *3*, 781−783.
79. Christopher, J. A. (1998) *SPOCK: The structural properties observation and calculation kit*, Texas A&M University, College Station, TX.

BI062139D